The RONSARD radars : a versatile C band dual Doppler facility

B. Nutten, P. Amayenc, M. Chong, Danièle Hauser, F. Roux, J. Testud

▶ **To cite this version:**

B. Nutten, P. Amayenc, M. Chong, Danièle Hauser, F. Roux, et al.. The RONSARD radars : a versatile C band dual Doppler facility. [Research Report] Note technique CRPE n° 69, Centre de recherches en physique de l'environnement terrestre et planétaire (CRPE). 1979, 36 p. hal-02191373

HAL Id: hal-02191373

https://hal-lara.archives-ouvertes.fr/hal-02191373v1

Submitted on 23 Jul 2019

HAL is a multi-disciplinary open access archive for the deposit and dissemination of scientific research documents, whether they are published or not. The documents may come from teaching and research institutions in France or abroad, or from public or private research centers.

L'archive ouverte pluridisciplinaire **HAL**, est destinée au dépôt et à la diffusion de documents scientifiques de niveau recherche, publiés ou non, émanant des établissements d'enseignement et de recherche français ou étrangers, des laboratoires publics ou privés.

RP 1812 (32)

CENTRE NATIONAL D'ETUDES DES TELECOMMUNICATIONS

CENTRE NATIONAL DE LA RECHERCHE SCIENTIFIQUE

CENTRE DE RECHERCHES EN PHYSIQUE DE L'ENVIRONNEMENT TERRESTRE ET PLANETAIRE

CRPE

NOTE TECHNIQUE
CRPE /69

the ronsard radars : a versatile c band dual doppler facility

LABORATOIRE DU CENTRE DE DOCUMENTATION C.N.E.T.

par
B. NUTTEN, P. AMAYENC, M. CHONG,
D. HAUSER, F. ROUX, J. TESTUD

CRPE/ETE
92131 ISSY LES MOULINEAUX

5 MARS 1980

CENTRE NATIONAL D'ETUDES
DES TELECOMMUNICATIONS

CENTRE NATIONAL DE LA
RECHERCHE SCIENTIFIQUE

NT/CRPE/69

THE RONSARD RADARS : A VERSATILE C BAND DUAL DOPPLER FACILITY

par

B. NUTTEN, P. AMAYENC, M. CHONG
D. HAUSER, F. ROUX, J. TESTUD

CRPE/ETE
38-40 rue du Général Leclerc
92131 - ISSY-les-MOULINEAUX

Le directeur adjoint du CRPE

I. REVAH

L'Ingénieur en Chef
chargé du département ETE

P. BAUER

Septembre 1979

ABSTRACT

In this paper the authors describe a system of two Doppler radars (the RONSARD system) operated for the study of precipitating clouds (fronts and convective storms).

In a first part, emphasis is placed on the system requirements concerning both transportability and flexibility, due to the wide range of atmosphere phenomena to be observed. These requirements lead to an original implementation of the aerial, to a special design of the receiving chain (dual polarization capability, wide dynamic range, absolute self calibration capability) and to the implementation of real time digital subsystems (Amplitude and Phase Memory, Ground clutter cancellor, Fourier Transform processor, Ambiguous Velocity corrector and a Spectrum Moment Computer).

The second part is devoted to a brief review of the scientific programs involving the RONSARD system and to the presentation of some preliminary results.

I - INTRODUCTION

RONSARD* is a versatile C band dual Doppler radar system operated by the Centre de Recherches en Physique de l'Environnement (CRPE), a common laboratory of Centre National de la Recherche Scientifique and Centre National d'Etudes des Télécommunications, for atmospheric studies**. Many pulse coherent radars have been described in the literature and, in some ways the RONSARD radars, whose main characteristics are given in table 1, are comparable to other equipments.

However, some unique characteristics of this system are worth being emphasized, particularly those concerning the installation and operating procedures, the receiver and the real time data processing unit.

It will be shown in section 1 that special care has been exercised to achieve transportability and reliability, the consequences of which have been a special aerial design and a fully digital signal processor. For instance, RONSARD uses magnetron transmitter and a digital phase memory instead of the conventional STALO-COHO method for obtaining coherence. In addition, high data compression requirement led to implementation of hardware real time digital susbsystems.

Section 2 is devoted to a brief review of the CRPE scientific programs based on the RONSARD system and to the presentation of a few preliminary results.

*Ronsard is an acronym for Recherche sur les Orages et les Nuages par un Système Associé de Radar Doppler.

**The RONSARD system, funded by the Délégation Générale à la Recherche Scientifique et Technique, the Centre National d'Etudes des Télécommunications and the Institut National d'Astronomie et de Géophysique, has been built by the Laboratoire Central de Télécommunications.

SECTION 1

A - RADAR CONFIGURATION

Each of the two identical radars consists of two transportable subsystems. One is a trailer (figure 1) supporting the fully steerable antenna as well as the transmitter and receiver boxes attached behind the antenna. The full azimuthal motion is limited to a 720° scan. This design eliminates all Radio Frequency (RF) and Intermediate Frequency (IF) rotary joints thus improving the reliability of the equipment.

The two V-shaped wings fixed behind the antenna are designed to dynamically balance the aerial against differential wind forces, thus reducing the necessary power and the weight of the servo-motors. The second part of each radar is a transportable shelter (figure 2) containing the control desk, the processor, and the on-line mini-computer.

The time needed to install the equipments on site, assuming that hard horizontal platforms are available, is of the order of three days for each radar ; it consists of assembling the antenna and wings, positioning the trailers, connecting cables, and testing the system.

B - PRINCIPAL CHARACTERISTICS OF THE RECEIVER

1. Dual polarization capability

A 450° K overall effective noise temperature measured at the antenna port is achieved by use of a two stage-120° K parametric amplifier. The additional noise is due to various wave guide losses between the feed horn and receiver caused by the dual polarization circuitry. Figure 3a shows the RF stages of the radar with an orthomode coupler and a polarization switch, controlled by the computer according to the timing diagram described in figure 4.

The switch selects vertical (V) or horizontal (H) polarization for the receiver while the transmitter polarization, mechanically fixed, can be switched manually by dismounting and reassembling RF circuitry (time needed for this operation : about 30').

2. Automatic gain control

A large dynamic range is obtained by the action of a fast Automatic Gain Control (AGC) achieving a "floating point" architecture whose exponent is the AGC factor. A 1 μs response time allows full gain control between two successive range gates. Thus AGC maintains the received echoe intensity within an interval approximately 9 dB wide. This is an important feature for dealing with the calibration problems. The AGC circuitry sets a 6 dB quantized PIN-diode attenuator, allowing 48 dB gain control. Moreover, when the echoe intensity approaches the saturation level, the parametric amplifiers are automatically switched-off, and their 30 dB gain is replaced by a 2 dB insertion loss. The total AGC dynamic range is increased to 80 dB, and the total linear receiver dynamic range is increased to more than 110 dB.

The timing of the AGC can be described as follows. The signal in each range gate is processed independently according to an elementary cycle of 64 transmitted pulses (22,44 or 88 ms depending upon the PRF). This cycle is divided into two phases :

Fast loop

During each of the first eight soundings of the cycle, the receiver gain is decreased of one (or two) 6 dB steps depending upon the signal intensity compared to two thresholds set equal to 6 dB and 0 dB under the saturation level of the coders. After this, the gain has been decreased of up to 80 dB.

Slow loop

From the 9^{th} to the 64^{th} sounding of the cycle, the gain is held in the range gate thus allowing a valid measurement of the intensity.. Simultaneously, an estimate of the mean signal intensity is computed in a digital video integrator.

Assuming that the 64 range gates are kept identical during the following cycle, the gain in the choosen gate is then kept constant or increased of one 6 dB step for the next cycle if the mean signal intensity is respectively over or under a threshold set 12 dB under the saturation level. So, taking advantage of signal stationnarity, the gain in each range gate is estimated from cycle to cycle according to the mean signal intensity, but is rapidly adjusted in cases of increasing reflectivities.
On the contrary, if the ranges of the observed gates differ during the following cycle, the AGC values are reset to zero (i.e. the gains in all range gates are initialized to their maximum value).

The RONSARD receiver extended dynamic range is illustrated in figure 5 showing power measurements obtained with an echo-box.

3. Self calibrating capability

Another interesting feature, which is important for reflectivity measurements, is the self-calibrating capability. Every 40 seconds, a known signal from a temperature stabilized source oscillating at the transmitter frequency (± 50 kHz) is fed to the input of the parametric amplifiers with a fixed AGC value. The power measurement at the output of the receiver is sent to the computer which controls a 6 dB PIN diode RF attenuator. This feed-back is designed to conterbalance the drift of various RF or IF amplifiers and keeps the overall gain constant (within .5 dB) when the external temperature varies between -20 to 50°C.

C - PRINCIPAL CHARACTERISTICS OF THE PROCESSOR

1. Complex video processor

The RONSARD processor is designed for handling complex video signals. After mixing with an RF local oscillator (fig 3a) the returned signal is mixed with the output of a free running 60 MHz oscillator (fig 3b), the frequency of which equals that of the receiver IF. This standard super-heterodyne design is modified since the IF signal is mixed with two IF oscillator outputs with 90° phase shift. Thus the two zero frequency signals delivered by the IF mixers can be considered as quadrature components (I and Q) of the complex video signal.

This design doubles the Nyquist frequency (f_r here instead of $f_r/2$ for classical pulsed Doppler radars) and retains the sign of the Doppler frequency.

2. Amplitude and phase memory

The standard coherent oscillation (COHO) of conventional Doppler radars with magnetron transmitters is replaced by a fully digital subsystem called the Amplitude and Phase Memory (APM) (figure 6). This APM performs both phase adjustment of the sampled complex video signal in each range gate and the correction of amplitude fluctuations of the transmitted signal :

A sample of the transmitted pulse is mixed with the local oscillator and connected to the IF mixers for 5 μs following the radar trigger. After this, the switch passes the returned signal to the mixers. Since the part of the transmitted pulse and the returned signal are processed by the same low-pass filters, the amplitude and phase fluctuations of the transmitted wave are eliminated, as well as the amplitude and phase of the returned intensity. In both cases, only one complex intensity value is obtained and is associated to the mean amplitude and phase of the signal (transmitted or received) during the range gate.

The computing time of this device, according to an algorithm detailed in fig. 6, is of course lower than the minimum 1 μs interval between two successive range gates. The APM is a reliable device due to its solid state design.

3. Ground clutter cancellor

Another subsystem of interest is a recursive digital filter designed to eliminate echoes from fixed targets. This low frequency canceller is implemented in the time domain in order to allow the recording for special purposes (see section 2, Soundings at vertical incidence) of filtered time series.

A multiplication in the frequency domain (after the discrete Fourier Transform), in spite of a lower cost, would not have offered that opportunity.

Three cut off frequencies (20, 40 or 60 Hz) and two slopes (40 or 80 dB/decade corresponding to a two or four poles transfer function) can be selected, and the whole circuit can be by-passed if necessary.

4. Approximate Fourier Transformer

An approximate Fourier Transformer, based on the DFT algorithm, can process the 64 points complex time series for 64 simultaneous range gates in 22 ms. This high performance is obtained by a coarse quantization of the sinus and cosinus functions in the table of the DFT. These functions take successively the following values : -1, -1/2, +1/2 and 1. So all multiplications of the true DFT are replaced by one-bits shifts thus increasing the computing speed of the device.

The effects of that quantization can be seen by considering that the unit circle is replaced by discrete points made with the 8 vertex of a circumscribed octagon (fig. 7a,b). The result is a 1.25 power gain and additive noise. However, spurious spectrum lines are maintained at least 13 dB below the main spectrum line amplitude. Prior to calculating the spectral moments, a threshold at -12 dB from the peak is used to guarantee that the clutter due to approximate DFT does not appear in the estimated signal spectrum. (Fig. 7c, d)

5. Moments computer

The data flow at the output of the analog-to-digital converters is about 3.0 M bit s^{-1} for highest PRF. This is the results of 64 dual conversions with 8 bits coders 2 928 times per sec.

After computation of the Power Spectrum Density when, thanks to the use of ping-pong memory, no data are missed, 64 power spectra of 64 x 10 bits lines are obtained every 22 ms. So the data flow remains about 1.9 Mbit s^{-1}, which is quite demanding for standard magnetic tape recorders. Data compression is achieved in a post-processor that computes the first three moments M_0, M_1 and M_2 of the PSD. Even after addition of some house-keeping data (time, antenna coordinates, AGC's) the data flow is reduced to 0.12 Mbit s^{-1} which is compatible with standard 20 K byte s^{-1} recorders acquisition rate.

The three moments and the AGC value in each range gate are used to compute both the reflectivity factor and the radial velocity of the scatterers.

The second moment of the PSD leads to a measurement of the spectrum variance which, until now, has mainly been used for elimination of spurious echoes. A variance threshold, adjusted to 5 $m^2 s^{-2}$ for treatment of frontal systems data, is used at this time for eliminating :

i - regions with no echo (radar noise only),

ii - multiple trip returns characterised by a high reflectivity factor and a white-noise type spectrum.

6. Ambiguous velocity corrector

The radial velocity and the velocity variance are derived from straightforward algorithms computing the mean frequency and variance of power spectra :

$$f = \frac{M_1}{M_2}$$

$$\sigma^2 = \frac{M_2}{M_0} - \left(\frac{M_1}{M_0}\right)^2$$, where M_i is the i^{th} spectral moment.

These estimators provide erroneous measurements of the mean velocity and variance when the central line of the spectrum approaches the limits of unambiguous domain as illustrated in the figure 8a :

- The mean velocity is found close to 0,
- The variance is significantly overestimated.

A real time subsystem, Ambiguous Velocity Corrector has been implemented to increase the post processor efficiency, for data approaching the limits of the velocity domain. It operates as follows : the overall zeroth order moment of the spectrum M_0 and the part of this moment M_0 contained in two spectral window (fig. 8a) containing the extreme lines of the spectrum are computed simultaneously according to the following equations :

$$M_0 = \sum_{-32}^{+31} S_i$$

$$M'_0 = \sum_{-32}^{-29} S_i + \sum_{28}^{+31} S_i$$

where S_i are the spectral lines of the PSD.

A $\frac{M'_0}{M_0} > k$ test (with $0 < k < 1$) is then used for detecting spectra where ambiguous velocity values are expected. In such a case, assuming f_r is the pulse repetition frequency, a $f_r/2$ shift is applied on the PSD lines before computing the first and second moments. This procedure allows a valid computation of the radial velocity and the variance (fig. 8b) if the folded spectrum is correctly detected. This subsystem is still under test with a $k = 0.5$ threshold.

PPP Versus DFT with threshold

The RONSARD radars project was started in 1972, just before the great development of Pulse Pair Processors (PPP) [2, 8], which can estimate spectral moments without calculating the complete Doppler spectrum. Analyzing the Fourier Transform (FT) with threshold and covariance techniques for frequency measurements [9], we find a definite superiority of PPP for low signal-to-noise ratios (< 0 dB) mainly due to the poor behavior of the FT technique when the spectrum central frequency approaches the Nyquist frequency.

In addition, thanks to its simpler algorithm offering an increased number of range gates at a lower cost, the second technique has subsequently grown to a wide extent in meteorological Doppler radars.

Yet, some points should be clarified, particularly concerning the PPP and FT behaviour when data with multiple peak spectra (eg spectra of meteorological echoes mixed with ground clutter, or multiple trip returns, are processed.

i - In case of multiple peak spectra, it clearly appears that both methods yield erroneous measurements of the radial velocity. It should be noticed however that the good estimate of the variance in the FT case allows a straightforward elimination of the spurious data.

On the contrary the variance estimator [2 , 9] most commonly used as well as the three lags estimator proposed recently [10 , 13] lead to an underestimated variance value. Thus the erroneous velocities caused by fixed echoes may not be detected as reliably as they can be with FT processing, if clutter suppression techniques are not employed.

Moreover, the PPP mean velocity estimator is sensitive even to a low intensity secondary peak in the spectrum. Thus, due to leakages of digital high pass filters, advantage cannot really be taken of fixed target canceller implementations. In any case, covariance argument techniques used for variance estimations imply an assumption concerning spectra shapes (usually "Gaussian") which is unacceptable in case of multi-mode spectra.

ii - When processing poor signal-to-noise ratio spectra, the velocity estimator based on FT technique has poor results mainly because of biasing at Nyquist interval. In case of RONSARD radars, this particular disadvantage is partly overcome since spectra approaching the Nyquist interval are detected and shifted (see § C.6).

However the disadvantage of FT method mainly appears when handling multiple trip returns mixed with unambiguous signals : the -12 dB threshold operated on such a spectrum is strongly exceeded since the multiple trip return behaves as an uncorrelated noise with high intensity, generaly yielding a very low signal-to-noise ratio.

The FT estimator delivers a close to zero velocity estimate while PPP has a correct radial velocity estimate if the signal-to-noise ratio keeps greater than 0 dB [9].
But, whatever is the origin of spectrum broadening (radar noise or multiple return echoes) the FT estimate of the variance exceeds the previously mentionned variance threshold and the associated mean velocity is eliminated. On the contrary, covariance argument variance estimators
cannot easily yield a coherent power test. This is a major advantage of FT technique which clearly appears when one attempt the integration of continuity equation in order to retrieve the tri-dimensional wind field from dual Doppler measurements (see section 2), since the method is very sensitive to spurious data.

The previous discussion leads to the conclusion that, in spite of low cost advantage, Pulse Pair Processors have deficiencies for certain types of data which Fourier Transform techniques with ambiguous velocity correctors naturally overcome (incorrect multiple peaksspectrum processing, deficient erroneous data rejection when handling multiple return echoes). The benefit of the Fourier transform technique, with its spurious data elimination capability, is however counterbalanced by higher complexity and cost.

SECTION 2

The flexibility of the RONSARD system is the result of both the radars design and of the special receiver and data processing. A short description of typical procedures for observing air motions, and various examples of preliminary scientific results are given below.

A - OBSERVATIONAL PROCEDURES

Three types of methodologies are used for investigation of the air motions and precipitation characteristics ; they correspond to three methods of analysis of the observational data.

1. Conical scanning (single radar methodology - Typical exploration time : 7 minutes)

Hemispherical exploration is performed through full 360° scannings at various fixed elevation angles and with typical ranges of .8 - 100 km. The method described by Browning-Wexler [4] , extended to the case of non uniform distributions of tracers [11] , is used for radial velocity analysis. It provides vertical profiles of the mean horizontal velocity $\overline{V}_H$ and divergence div $\overline{V}_H$ at scales of about 40 km. In addition, the vertical velocity may be obtained by the integration of the continuity equation under the anelastic approximation. This method was used in observations of stratiform precipitation associated with frontal systems [11] .

Figure 9 shows the horizontal wind field in the vicinity of a cold front as deduced from the conical scanning methodology. Isocontours of cross front velocity (upper diagram) and long front velocity (lower diagram) are displayed in a reference frame moving with the front.

Ahead of the front, the mixing of the two air masses is found associated with ageostrophic motions with significant horizontal accelerations and with intense vertical ascent. The rain bands are found stationary in the frame moving with the front.

2. Coplan (Dual radar methodology - Typical exploration time : 3 minutes)

This classical methodology, adapted for investigation of three dimensional convective motions associated with storms or showers, was first proposed by Lhermitte [7]. The interpolation program (needed to analyze dual Doppler data on a common grid) that is used with RONSARD data yields a three dimensional wind field over a typical 50 x 50 x 10 km volume with a resolution of 1 x 1 x .5 km. This basic technique has been improved to allow a correct retrieval of the first derivative of the wind field which leads to the computation of the vertical air acceleration derived from standard hydrodynamic equations and thus to the buoyancy force.

Figure 10 illustrates the convective wind field observed in a shower using the coplan methodology. A vertical cross section of the wind field is exhibited, superimposed on isocontours of the vertical acceleration.

3. Soundings at vertical incidence (single radar methodology - Typical resolution range : minimum altitude = 800 m, altitude resolution = 200 m - Typical time needed for a 10 km altitude range acquisition : about 0.5 s)

Taking advantage of the 64 point samples time series recording capability, an off line Fourier processor yields power spectrum densities with about 30 dB dynamic range. An objective noise level determination [6] is used to set the threshold.

At vertical incidence, the PSD essentially represents the terminal fall velocity spectrum of hydrometeors shifted by the mean vertical air velocity. Assuming the drop size distribution of hydrometeors to be of the form $N(D) = N_0 \exp(-\Lambda D)$, a new technique, based on a three parameters non linear least square fitting has been developped allowing simultaneous estimates of :

- the slope and intercept parameters of the distribution Λ and N_0,
- the vertical air velocity W.

Briefly, each observed Doppler spectrum is fitted by a theoretical curve depending on the three previously described parameters which are adjusted until the mean square deviation between the two spectra becomes minimum. Details on this method will be fully given in a future paper presently under progress.

Figure 11 shows vertical profiles of :

i - parameters of the doppler spectrum (reflectivity factor Z, mean radial velocity $< v >$, velocity standard deviation σ) ;

ii - results of the least square fitting analysis in N_0, Λ and W (The corresponding water content is also indicated).

This figure clearly displays the transition between water and ice particles near the altitude of the 0° isotherm, just above the classical feature of the bright band. Notice also that the growth of precipitation is observed above 4 km altitude in the ice phase.

B - CRPE SCIENTIFIC PROGRAM

The radars are engaged in CRPE scientific programs generally involving other atmospheric research laboratories or the Meteorological Office, so that the necessary environmental data (radiosoundings, satellite imagery, raingauges, radio link measurement) are available. The activity is organized around three main topics :

1 - Air Dynamics, and the physics of precipitation in mid-latitude frontal systems. The use of the three previous methodologies provides dynamical data in a wide scale range (from 1 to about 300 km) and microphysical information from vertical incidence soundings allow the study of the formation process of precipitation.

2 - Dynamics, thermodynamics and precipitation associated with deep convection. Coplane methodology and occasionally vertical incidence soundings are used, yielding the three-dimensional wind vector, precipitation field, and microphysical data. This leads to a better knowledge of the formation process of precipitation in convective conditions, and of the interaction

between air dynamics and precipitation. In addition, the estimation of vertical fluxes of momentum, mass, vorticity, liquid water, which is possible from our data allows an approach to the problem of convection parametrization.

3 - Propagation studies in the frequency range 4 - 14 GHz for Telecommunication purposes. This program is based on the simultaneous use of dual polarization radar data, and data of attenuation or cross polarization obtained on radio links (11 and 14 GHz beacons of the O.T.S. satellite, and 4 to 13 GHz terrestrial radio links). The radar data are used both to determine the structure of rain cells aloft and to identify the hydrometeors responsible for the cross polarizing and attenuating properties of the precipitation.

A frontal observation program started in spring 76 near Paris and continued in Oct-Nov 77 and March 78 with observation campaigns involving others atmospheric laboratories [5].

First deep convection observations took place in Switzerland (1978). Future development of the convection program is based on a French cooperative experiment , near Bordeaux in July-August 79 which also involves extensive measurements of electric field [3].

Tropical convection will be investigated in May and June 81 in an Ivory Coast experiment [1].

FIGURES

Figure 1 : A RONSARD radar trailer which supports the aerial, transmitter and receiver.

Figure 2 : A RONSARD setup showing antenna and shelter.

Figure 3 : RONSARD block diagram (a : trailer b : shelter).

Figure 4 : RONSARD typical dual polarization sequence for the measurement of the orthogonal components of the scattered field (the transmitted field is linearly polarized and not switched). A minimum 60 ms switching time is needed between observation periods T.

Figure 5 : AGC response to a rapidly varying signal with wide dynamic range. The feed horn has been replaced by a C-band echo box through an isolating 10 dB attenuator. The returned power from a transmitted pulse is a strong signal observed at a .8 km distance rapidly decreasing to a value lower than the receiver noise after 4 km. Curve (a) shows the measured power after the gain control. Curve (b) shows the AGC attenuation values and curve (c) the retrieved power received from the echo-box.

Figure 6 : Amplitude and phase memory subsystem (APM).
After mixing the IF returned signal with two quadrature 60 MHz local oscillator outputs, the measured complex signal has to be corrected depending upon the mean amplitude and phase of the transmitted pulse. Let us assume that $\overline{OP}_o$ is the representative vector of the transmitted pulse (with phase φ_o, amplitude A_o, X_o and Y_o as I and Q coordinates)and that $\overline{OP}_i$ is the received signal in each of the 64 range gates (with phase φ_i and amplitude A_i, X_i and Y_i as I and Q coordinates).

The APM operation is equivalent to a complex division of all $\overline{OP}_i$ vectors by $\overline{OP}_o$. The $\overline{OP'}_i$ representative points of the video signals at the output of the APM are thus defined by the following equations :

$$\overline{OP'}_i = \frac{\overline{OP}_i}{\overline{OP}_o} \qquad \left| \begin{array}{l} X'_i = \dfrac{X_i X_o + Y_i Y_o}{X_o^2 + Y_o^2} \\ Y'_i = \dfrac{Y_i X_o - X_i Y_o}{X_o^2 + Y_o^2} \end{array} \right.$$

Figure 7 : The approximate Discrete Fourier Transformer.
Diagram (a) shows how the unit circle is approximated for the quantization of the sine and cosine tables and curves (b) are the display of sine and cosine values versus phase angle.
Figure (c) and (d) are power spectrum density representations obtained with a true DFT (c) and an approximate DFT (d) applied to the same sine wave. All spurious lines are lower than 13 dB below the main line level.

Figure 8 : Ambiguous Velocity corrector (AVC)

a) displays a typical folded power spectrum density obtained with RONSARD radars. The presence of energy close to the ambiguous values is detected in the Ambiguous Velocity Windows when computing the power spectrum density (PSD).

b) shows the same power spectrum density after a $f_r/2$ Doppler shift (which can be obtained by simply inverting the most significant bit of the PSD memory address) implemented before calculating the moments. The whole operation amounts to shifting the Fourier analysis window position according to the observed Doppler shift.

Figure 9 : Horizontal circulation inferred from single Doppler radar data. Isocontours of cross front velocity (upper diagram) and long front velocity (lower diagram) have been derived from 18 $\overline{V}_H$ vertical profiles obtained at the times indicated by triangles. Horizontal axis represents also horizontal distances assuming the stationarity of the flow and a front speed of 8 ms^{-1}.

Figure 10 : Vertical cross-section of the wind field. Corresponding isocontours of the vertical acceleration ($\gamma_Z = \overline{V}.\overline{\nabla}w - \overline{V}$ wind vector, w vertical velocity) are also shown.

Figure 11 : Mean results obtained from vertical sounding (during 90 s) in a large scale continuous precipitation associated to a warm front, near Paris. From left to right :

Z reflectivity factor, <V> mean Doppler velocity, σ standard deviation of the spectrum, Λ and N_0 parameters of the hydrometeors distributions, M precipitating water content, and W air vertical velocity (negative upward). Eventhough the two sequences of measurement are not obtained exactly at the same time, the successive results in altitude have been connected for clarity of the figure.

Also are indicated the altitudes of 0°C, -5°C and -10°C isotherms.

Table 1 : RONSARD radars main characteristics.

REFERENCES

[1] *Achy, S. , P. Amayenc, J.P. Chalon, M. Desbois, M. Gilet, P. Olory, C. Pastre, G. Sommeria, J. Testud : Avant projet d'une expérience d'étude de la convection profonde tropicale (COPT), Presentation report by CRPE, LMD, EERM and Abidjan University, 1978.

[2] Benham, F.C., H.L. Groginsky, A.S. Soltes and G. Works, 1972 : Pulse pair estimation of Doppler spectrum parameters. Final Report, Contract F - 19 628 - 71 - C - 0126, Raytheon Company, Wayland, Mass.

[3] *Boulay, J.L., M. Payen, G. Sommeria, P. Vangrunderbeck, S. Chauzy, P. Laroche, J. Testud : objectifs et organisation générale de l'expérience "Landes 79", Presentation report by CRPE, LMD, Météorologie nationale, L.P.A., CESTA, ONERA, 1979.

[4] Browning, K.A. and R. Wexler, 1968 : The determination of kinematic properties of a wind field using Doppler radar. J. Appl. Meteor., 7, 105-113.

[5] Gilet, M., Campagne de mesures "Fronts 77", Compte-rendu des opérations, Note technique EERM 407, April 1978, Météorologie Nationale - Paris.

[6] Hildebrand, P.H. and R.S. Sekhon, 1974 : Objective determination of noise level in Doppler spectra, J. Appl. Meteor., 13, 808-811.

[7] Lhermitte, R.M., 1970 : Dual Doppler observation of convective storm circulation, Preprints 14th Radar Met. Conf., Tucson, Americ. Meteor. Soc. 139-144.

[8] Miller, K.S. and M.M. Rochwarger, 1972 : A covariance approach to spectral moment estimation. IEEE Trans. Inform. Theory, IT-18, 588-596.

[9] Sirmans, D. and B. Bumgarner, 1975 : Numerical comparison of five mean frequency estimators, J. Apl. Meteor., 14, 991-1003.

[10] Srivastava, R.C., A.R. Jameson and P.H. Hildebrand, 1978 : Time-domain computation of mean and variance of Doppler spectra. 18th Conf. on Radar Meteorology, Atlanta, Ga, Amer. Meteor. Soc., 383-386.

[11] Testud, J., G. Breger, P. Amayenc, M. Chong, B. Nutten, A. Sauvaget, 1979 : A Doppler radar observation of a cold front : three-dimensional air circulation, related precipitation system, and associated wave like motions. Submitted to J. Atmos. Sci., 1979.

[12] Waldteufel, P. H. Corbin, 1979 : On the analysis of single Doppler Radar data. J. Appl. Met., 1979, 18, 532-542.

[13] Zrnic, D.S., 1979 : Spectrum width estimates for weather echoes. IEEE Trans. Aerosp. Electron. Syst.

*available on request at CNET/CRPE 38 rue du Général Leclerc
92130 ISSY-LES-MOULINEAUX

CHARACTERISTICS OF RONSARD RADARS

Table 1 1/2

TRANSMITTER

Frequency	f = 5 600 or 5 630 MHz ($\lambda \sim$ 5.4 cm/C Band)		
Type	coaxial magnetron with AFC		
Peak power	250 KW		
3 pulse repetition frequencies (Hz)	2 928	1 464	732
Pulse duration (μs)	.34	.68	1.36
Velocity span (Nyquist interval (ms^{-1})	78.2	39.1	19.6
Range (km)	50.4	101.6	204.0

AERIAL

Type	Cassegrain with circular paraboloïd main reflector
Diameter	4 m
Angular width (3 dB, one way)	.9 degree
On-axis gain	44.4 dB with 50 % efficiency
Maximum angular velocity	18° s^{-1}
Maximum acceleration	18° s^{-2}
Azimuth span	± 360°
Elevation span	-1/90°
Pointing accuracy	0.1 degree
Wind tolerance	60 km/hr (nominal), 140 km/hr (survival)

RECEIVER

Polarization	linear, horizontal or vertical
Recovery time	5.3 μs
Noise temperature	450° K (Noise figure : 4 dB)

Self calibrating capability

Quantized 6 dB AGC loop with overall 80 dB dynamic

Sensitivity Time Control system limited to a 24 dB interval.

Table 1 2/2

REAL TIME PROCESSOR

Switchable ground clutter canceller

. cut-off velocity : .5, 1, 1.5 ms^{-1}

. Number of poles in the transfert function : 2 or 4

Discrete Fourier Transform Processor with quantized sine and cosine tables.

Spectrum moments computer

Ambiguous velocities controller

RADAR MANAGEMENT SYSTEM

Mini computer based (MITRA 15) performing :

. Radar data acquisition
. Magnetic tape radar and house-keeping data recording
. Antenna motion management
. Interactive radar programming

DATA RATES (Range resolution volumes/sec)

1 - Time series recording

PRF	2928	1464	732
# range cells/sec	92	92	46

2 - FT processing

PRF	2928	1464	732
# range cells/sec	2928	1464	732

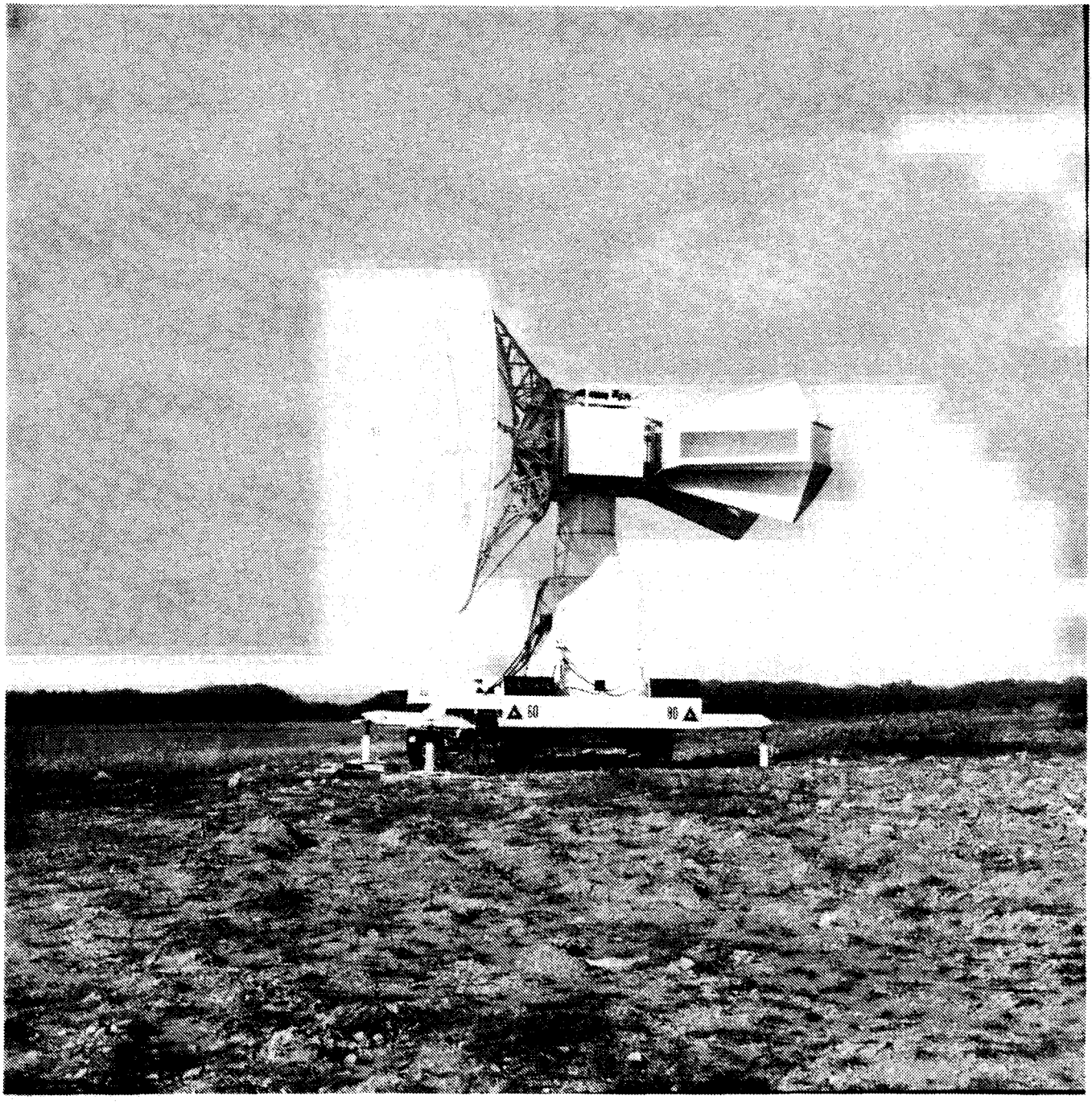

Fig. 1

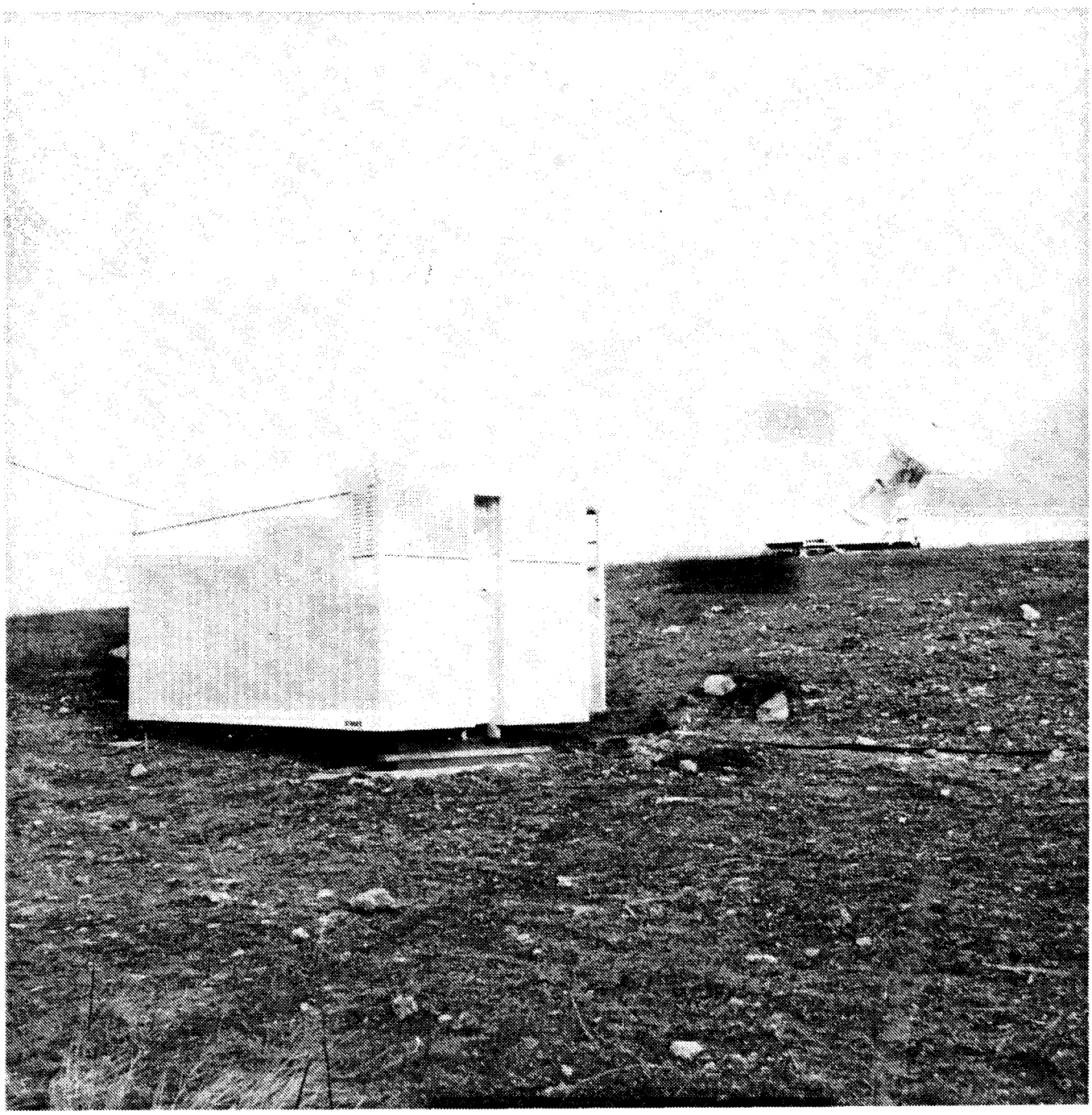

Fig. 2

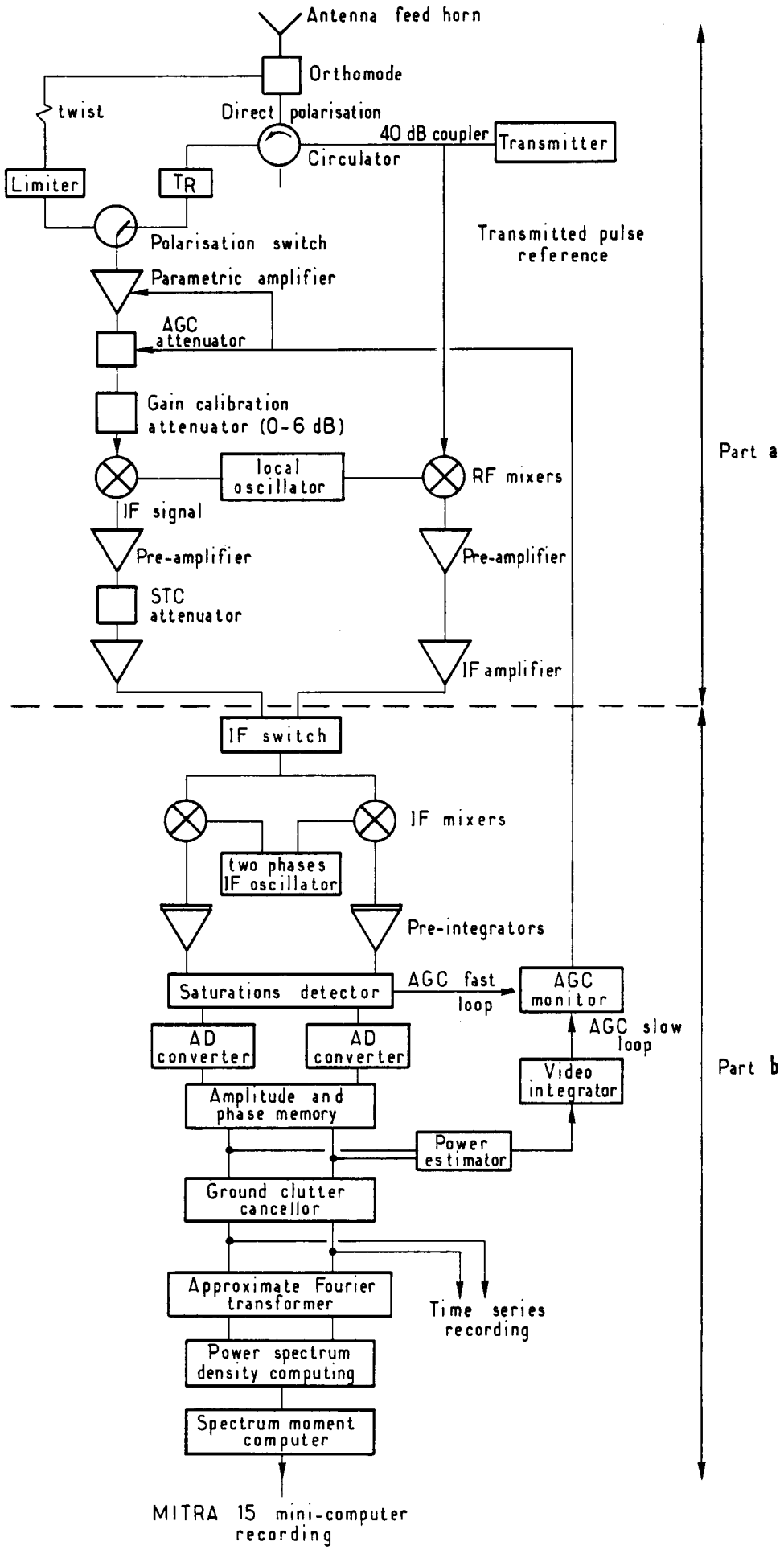
Antenna feed horn
Orthomode
twist
Direct polarisation
40 dB coupler
Transmitter
Circulator
Limiter
TR
Polarisation switch
Transmitted pulse reference
Parametric amplifier
AGC attenuator
Gain calibration attenuator (0-6 dB)
local oscillator
RF mixers
IF signal
Pre-amplifier
Pre-amplifier
STC attenuator
IF amplifier
Part a
IF switch
IF mixers
two phases IF oscillator
Pre-integrators
Saturations detector
AGC fast loop
AGC monitor
AD converter
AD converter
AGC slow loop
Video integrator
Amplitude and phase memory
Power estimator
Ground clutter cancellor
Approximate Fourier transformer
Time series recording
Power spectrum density computing
Spectrum moment computer
MITRA 15 mini-computer recording
Part b

Fig. 3

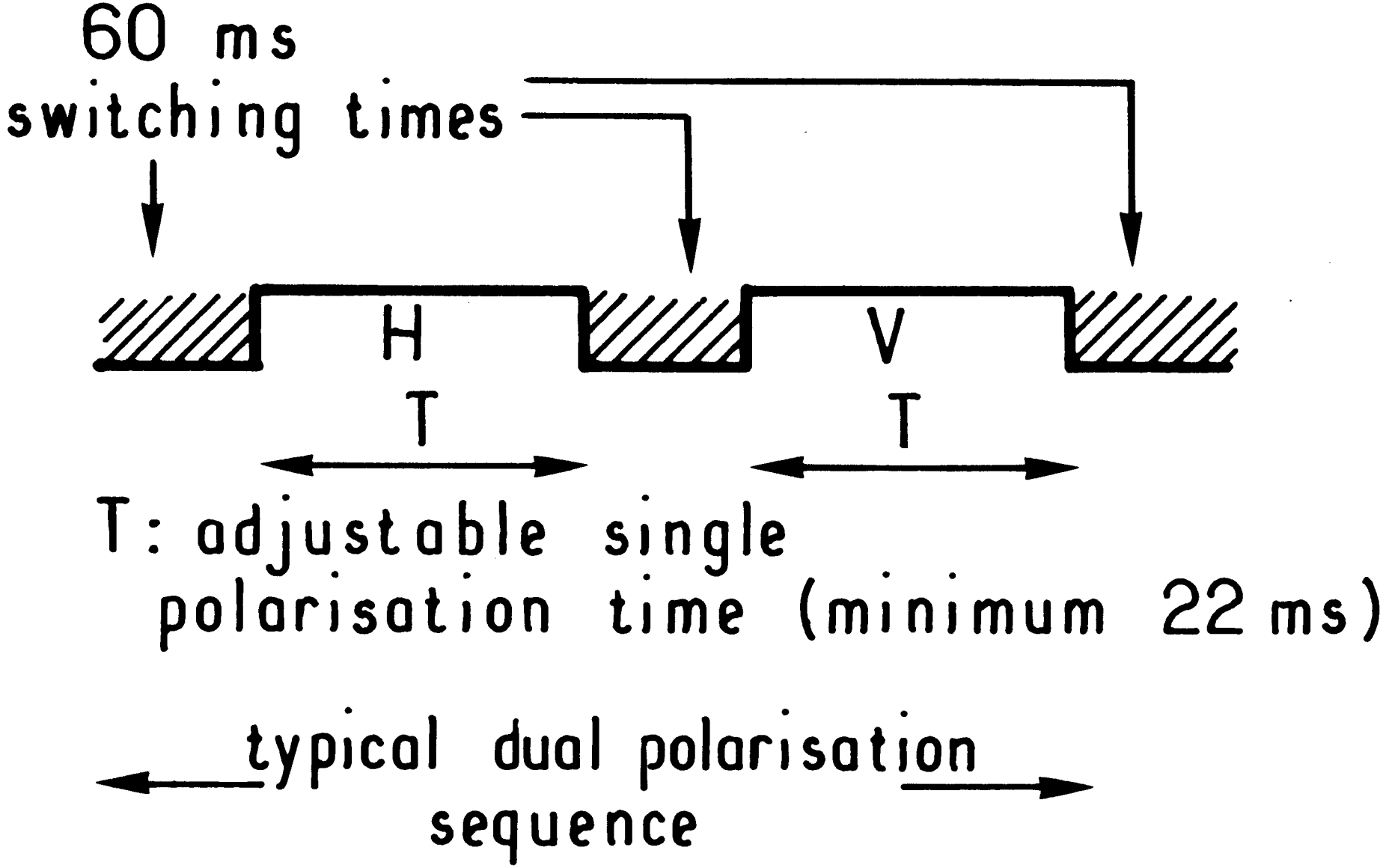
60 ms
switching times
H
V
T
T
T: adjustable single
polarisation time (minimum 22 ms)
typical dual polarisation
sequence

Fig. 4

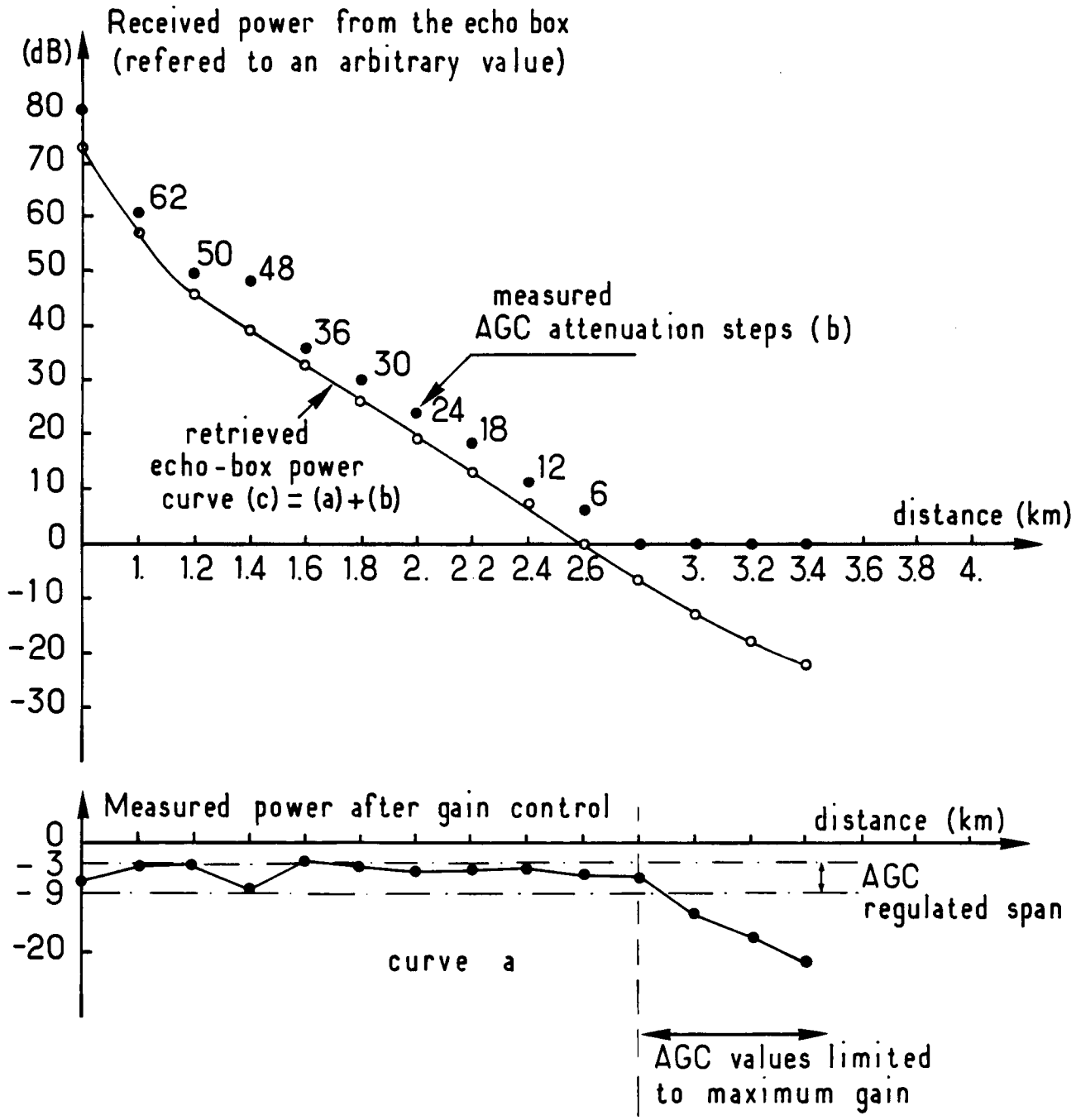
Received power from the echo box
(refered to an arbitrary value)
(dB)
80
70
60
50
40
30
20
10
0
-10
-20
-30
62
50
48
36
30
24
18
12
6
measured
AGC attenuation steps (b)
retrieved
echo-box power
curve (c) = (a)+(b)
distance (km)
1.
1.2
1.4
1.6
1.8
2.
2.2
2.4
2.6
3.
3.2
3.4
3.6
3.8
4.
Measured power after gain control
distance (km)
0
- 3
- 9
-20
AGC
regulated span
curve a
AGC values limited
to maximum gain

Fig. 5

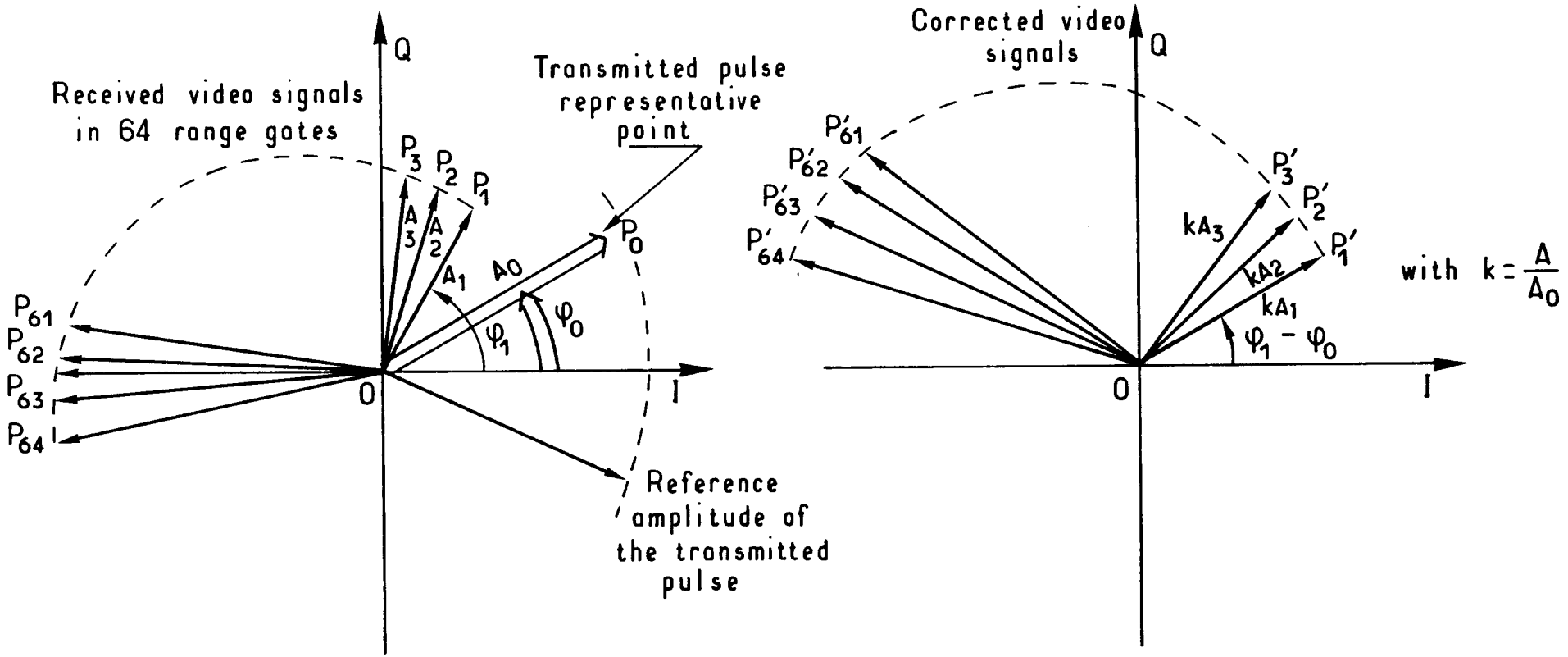
Received video signals in 64 range gates
Q
I
0
P61
P62
P63
P64
P3
P2
P1
A3
A2
A1
A0
φ1
φ0
Transmitted pulse representative point
P0
Reference amplitude of the transmitted pulse
Corrected video signals
P'61
P'62
P'63
P'64
P'3
P'2
P'1
kA3
kA2
kA1
φ1 - φ0
with k = A/A0

Fig. 6

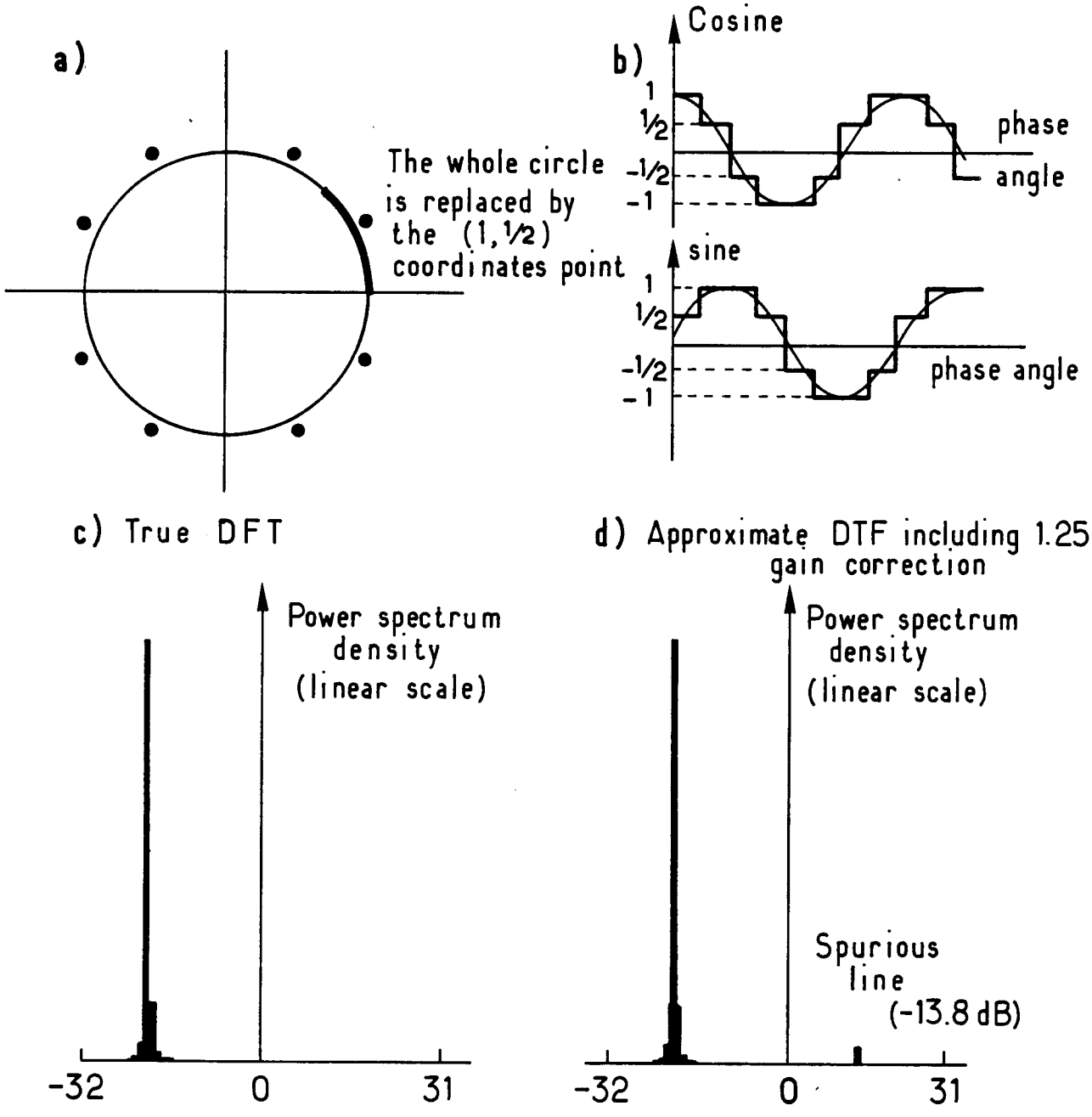
a)
The whole circle is replaced by the (1, 1/2) coordinates point
b)
Cosine
1
1/2
-1/2
-1
phase angle
sine
1
1/2
-1/2
-1
phase angle
c) True DFT
Power spectrum density (linear scale)
-32
0
31
d) Approximate DTF including 1.25 gain correction
Power spectrum density (linear scale)
Spurious line (-13.8 dB)
-32
0
31

Fig. 7

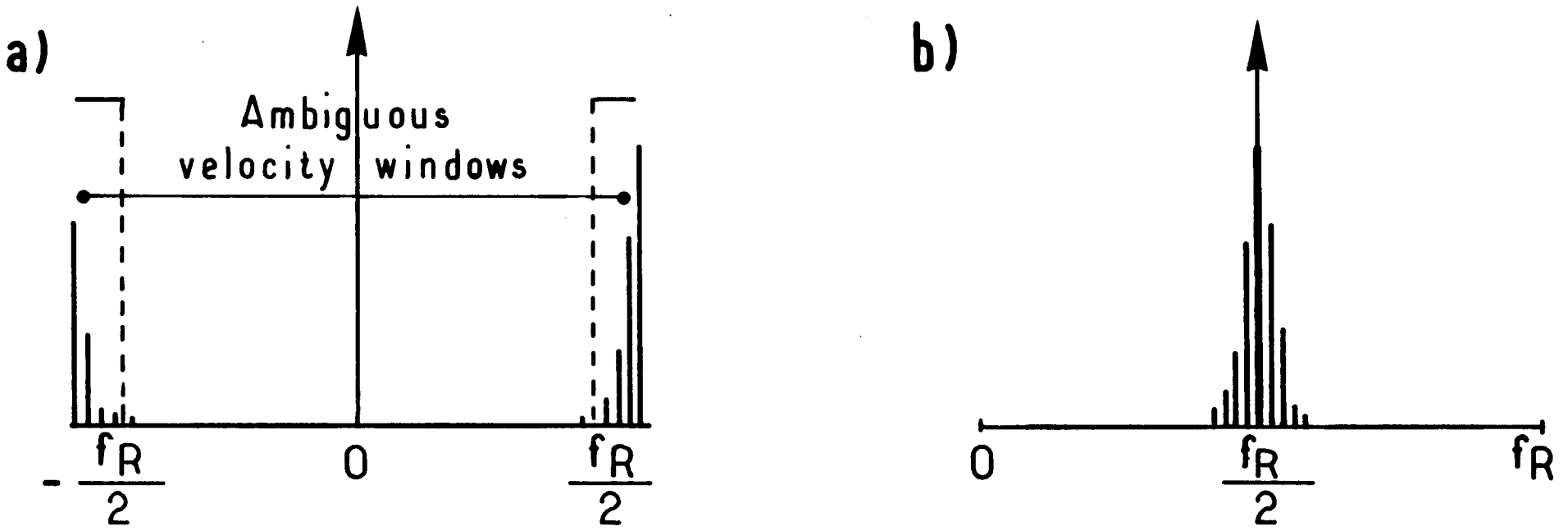
a)
Ambiguous
velocity windows
$-\frac{f_R}{2}$
0
$\frac{f_R}{2}$
b)
0
$\frac{f_R}{2}$
f_R

Fig. 8

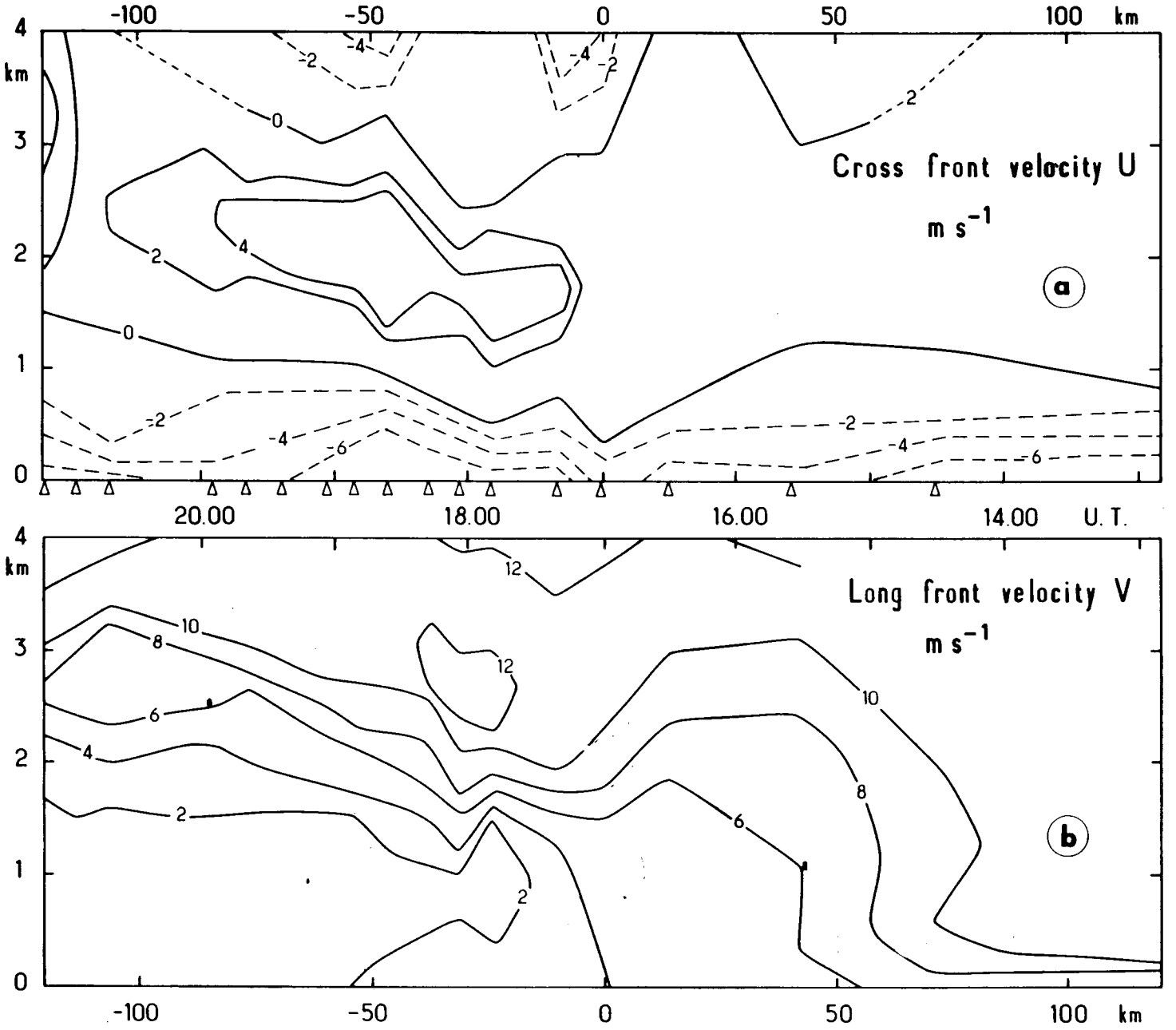
-100
-50
0
50
100 km
4
km
3
2
1
0
Cross front velocity U
m s-1
a
20.00
18.00
16.00
14.00 U.T.
Long front velocity V
m s-1
b

Fig. 9

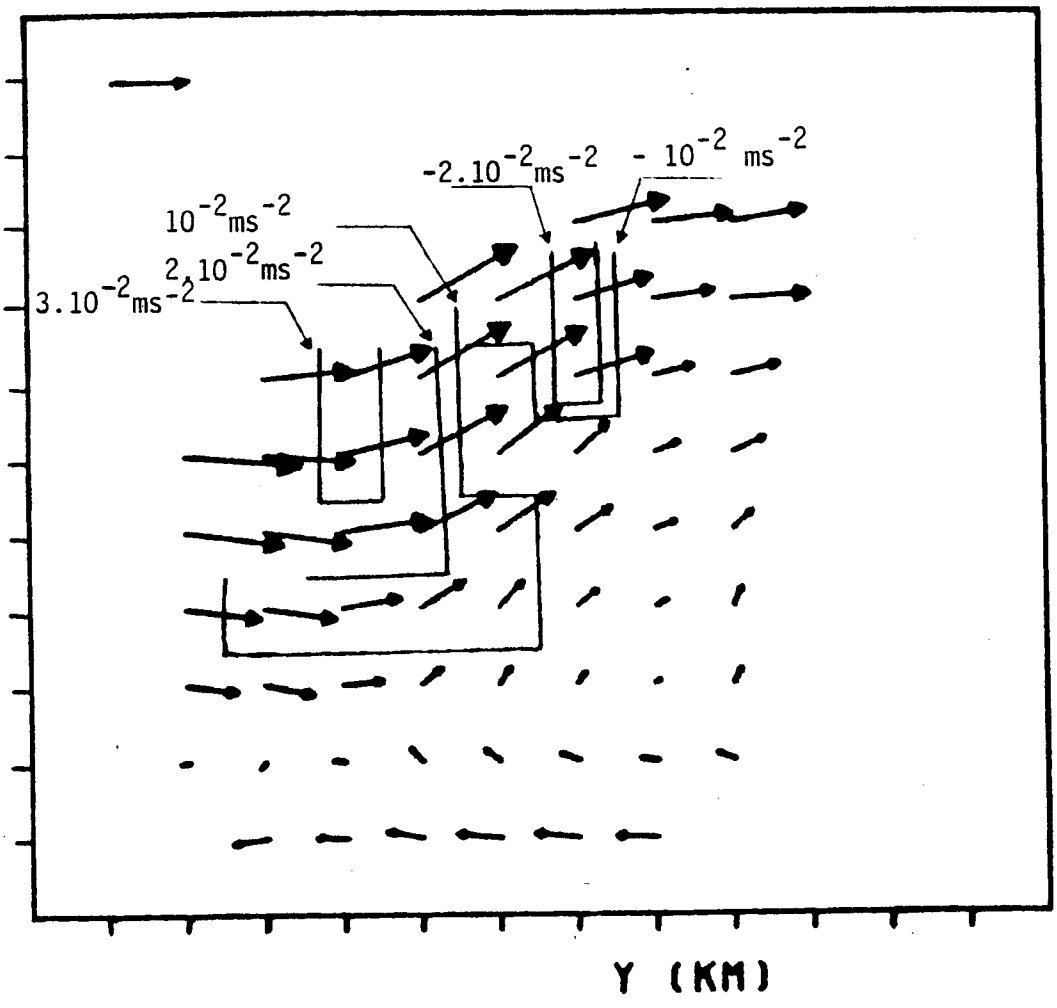

Fig. 10

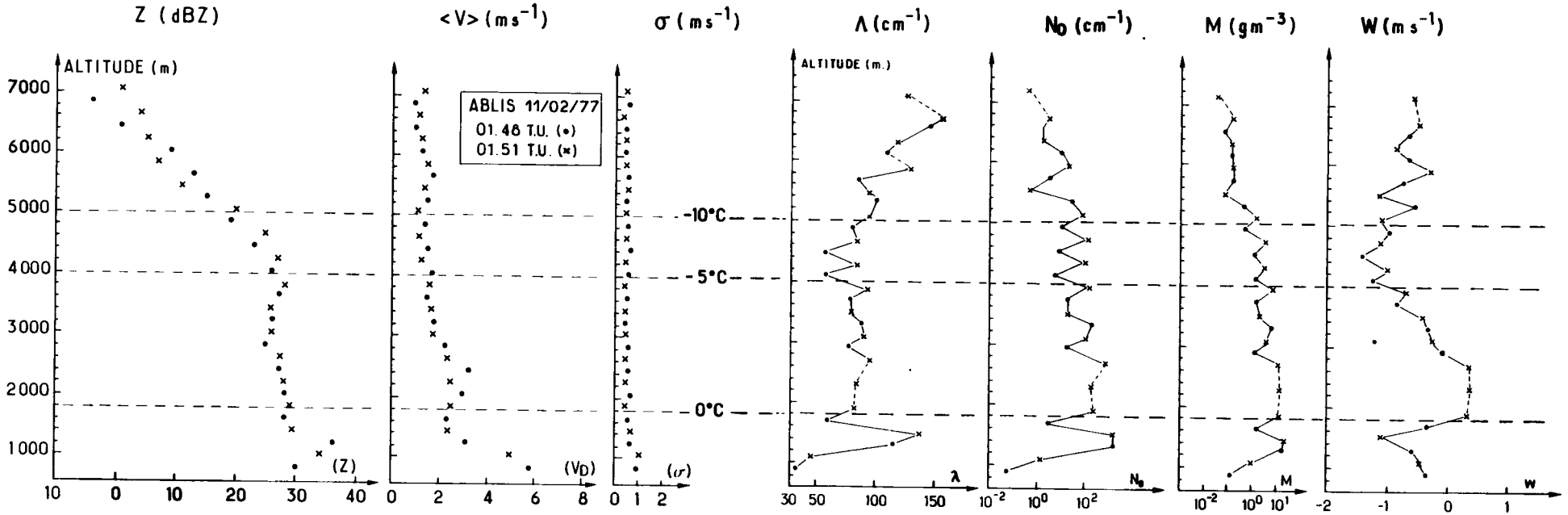
Z (dBZ)
<V> (ms⁻¹)
σ (ms⁻¹)
Λ (cm⁻¹)
N0 (cm⁻¹)
M (gm⁻³)
W (ms⁻¹)
ALTITUDE (m)
ABLIS 11/02/77
01.46 T.U. (•)
01.51 T.U. (×)
-10°C
-5°C
0°C
(Z)
(VD)
(σ)
λ
N0
M
W

Fig. 11

CRPE
Centre de Recherches
en Physique de l'Environnement
terrestre et planétaire

Avenue de la Recherche scientifique
45045 ORLEANS CEDEX

Département PCE
Physique et Chimie
de l'Environnement

Avenue de la Recherche scientifique
45045 ORLEANS CEDEX

Département ETE
Etudes par Télédétection
de l'Environnement

CNET - 38-40 rue du général Leclerc
92131 ISSY-LES-MOULINEAUX

CNET imp 75/1163